Group-velocity-dispersion measurements of atmospheric and combustion-related gases using an ultrabroadband-laser source

Paul J. Wrzesinski,[1] Dmitry Pestov,[2] Vadim V. Lozovoy,[1] James R. Gord,[3] Marcos Dantus,[1,2] and Sukesh Roy[4,*]

[1]*Department of Chemistry, Michigan State University, East Lansing, Michigan 48823, USA*
[2]*Biophotonic Solutions Inc., 1401 East Lansing Drive, Suite 112, East Lansing, Michigan 48823, USA*
[3]*Air Force Research Laboratory, Propulsion Directorate, Wright-Patterson AFB, Ohio 45433, USA*
[4]*Spectral Energies LLC, 5100 Springfield Street, Suite 301, Dayton, Ohio 45431, USA*
*sroy@woh.rr.com

Abstract: The use of femtosecond-laser sources for the diagnostics of combustion and reacting-flow environments requires detailed knowledge of optical dispersive properties of the medium interacting with the laser beams. Here the second- and third-order dispersion values for nitrogen, oxygen, air, carbon dioxide, ethylene, acetylene, and propane within the 700–900 nm range are reported, along with the pressure dependence of the chromatic dispersion. The effect of dispersion on axial resolution when applied to nonlinear spectroscopy with ultrabroadband pulses is also discussed.

©2011 Optical Society of America

OCIS codes: (320.7100) Ultrafast measurements; (320.5540) Pulse shaping; (260.2030) Dispersion; (120.1740) Combustion diagnostics.

References and links

1. S. Roy, P. Kinnius, R. Lucht, and J. Gord, "Temperature measurements in reacting flows by time-resolved femtosecond coherent anti-Stokes Raman scattering (fs-CARS) spectroscopy," Opt. Commun. **281**(2), 319–325 (2008).
2. S. Roy, W. D. Kulatilaka, D. R. Richardson, R. P. Lucht, and J. R. Gord, "Gas-phase single-shot thermometry at 1 kHz using fs-CARS spectroscopy," Opt. Lett. **34**(24), 3857–3859 (2009).
3. J. D. Miller, M. N. Slipchenko, T. R. Meyer, H. U. Stauffer, and J. R. Gord, "Hybrid femtosecond/picosecond coherent anti-Stokes Raman scattering for high-speed gas-phase thermometry," Opt. Lett. **35**(14), 2430–2432 (2010).
4. S. Roy, P. Wrzesinski, D. Pestov, T. Gunaratne, M. Dantus, and J. R. Gord, "Single-beam coherent anti-Stokes Raman scattering spectroscopy of N_2 using a shaped 7 fs laser pulse," Appl. Phys. Lett. **95**(7), 074102 (2009).
5. P. J. Wrzesinski, D. Pestov, V. V. Lozovoy, B. Xu, S. Roy, J. R. Gord, and M. Dantus, "Binary phase shaping for selective single-beam CARS spectroscopy and imaging of gas-phase molecules," J. Raman Spectrosc. (preprint), http://onlinelibrary.wiley.com/doi/10.1002/jrs.2709/abstract.
6. S. Diddams and J. Diels, "Dispersion measurements with white-light interferometry," J. Opt. Soc. Am. B **13**(6), 1120–1129 (1996).
7. R. Chlebus, P. Hlubina, and D. Ciprian, "Direct measurement of group dispersion of optical components using white-light spectral interferometry," Opto-Electron. Rev. **15**(3), 144–148 (2007).
8. M. G. Welch, C. E. de Nobriga, R. A. Correa, W. J. Wadsworth, and J. C. Knight, "Accurate measurement of the dispersion of hollow-core fibers using a scalable technique," Opt. Express **17**(11), 9006–9012 (2009).
9. A. G. Van Engen, S. A. Diddams, and T. S. Clement, "Dispersion measurements of water with white-light interferometry," Appl. Opt. **37**(24), 5679–5686 (1998).
10. T. D. Scarborough, C. Petersen, and C. J. G. J. Uiterwaal, "Measurements of the GVD of water and methanol and laser pulse characterization using direct imaging methods," N. J. Phys. **10**(10), 103011 (2008).
11. Y. Coello, V. Lozovoy, T. Gunaratne, B. Xu, I. Borukhovich, C. Tseng, T. Weinacht, and M. Dantus, "Interference without an interferometer: a different approach to measuring, compressing, and shaping ultrashort laser pulses," J. Opt. Soc. Am. B **25**(6), A140–A150 (2008).
12. Y. Coello, B. Xu, T. L. Miller, V. V. Lozovoy, and M. Dantus, "Group-velocity dispersion measurements of water, seawater, and ocular components using multiphoton intrapulse interference phase scan," Appl. Opt. **46**(35), 8394–8401 (2007).
13. A. M. Weiner, J. P. Heritage, and E. M. Kirschner, "High-resolution femtosecond pulse shaping," J. Opt. Soc. Am. B **5**(8), 1563–1572 (1988).

14. A. M. Weiner, "Femtosecond pulse shaping using spatial light modulators," Rev. Sci. Instrum. **71**(5), 1929 (2000).
15. J. Dymond, *The Virial Coefficients of Pure Gases and Mixtures: A Critical Compilation* (Clarendon and Oxford University Press, 1980).
16. A. Börzsönyi, Z. Heiner, M. P. Kalashnikov, A. P. Kovács, and K. Osvay, "Dispersion measurement of inert gases and gas mixtures at 800 nm," Appl. Opt. **47**(27), 4856–4863 (2008).
17. T. A. Pitts, T. S. Luk, J. K. Gruetzner, T. R. Nelson, A. McPherson, S. M. Cameron, and A. C. Bernstein, "Propagation of self-focusing laser pulses in atmosphere: experiment versus numerical simulation," J. Opt. Soc. Am. B **21**(11), 2008–2016 (2004).
18. I. Pastirk, X. Zhu, R. M. Martin, and M. Dantus, "Remote characterization and dispersion compensation of amplified shaped femtosecond pulses using MIIPS," Opt. Express **14**(19), 8885–8889 (2006).
19. K. Osvay, Á. Börzsönyi, A. Kovács, M. Görbe, G. Kurdi, and M. Kalashnikov, "Dispersion of femtosecond laser pulses in beam pipelines from ambient pressure to 0.1 mbar," Appl. Phys. B **87**(3), 457–461 (2007).
20. H. Li, D. A. Harris, B. Xu, P. J. Wrzesinski, V. V. Lozovoy, and M. Dantus, "Coherent mode-selective Raman excitation towards standoff detection," Opt. Express **16**(8), 5499–5504 (2008).
21. H. Li, D. A. Harris, B. Xu, P. J. Wrzesinski, V. V. Lozovoy, and M. Dantus, "Standoff and arms-length detection of chemicals with single-beam coherent anti-Stokes Raman scattering," Appl. Opt. **48**(4), B17–B22 (2009).

1. Introduction

Developments in the optical diagnostics of combustion and reacting-flow environments have been closely linked to advances in ultrafast-laser technology. Historically, this field of study has been dominated by the use of nanosecond (10^{-9} sec) and picosecond (10^{-12} sec) sources. However, femtosecond (10^{-15} sec)-laser sources have recently been successfully applied for gas thermometry [1–3], pressure studies [4], and imaging of turbulent gas flows [5]. While these experiments reinforce the numerous advantages of broadband-laser sources and optical diagnostics on the femtosecond time scale, they also bring attention to an inherent nuance of ultrashort (spectrally broadband)-pulse propagation–femtosecond pulses are much more susceptible to temporal broadening due to group-velocity dispersion (GVD) than picosecond and nanosecond pulses.

The GVD of many solids [6–8] and liquids [9,10] have been measured with several experimental methods. However, GVD information for gas phase molecules is not as prevalent. In this study we focus on the dispersion properties of common atmospheric and combustion gases at room temperature and explored their scalability with gas pressure. We relied on the Multiphoton Intrapulse Interference Phase Scan (MIIPS) technique [11] to obtain the chromatic dispersion of these gases over the 700–900 nm range, limited by the spectral bandwidth of our laser. MIIPS directly measures the second derivative of the pulse spectral phase, $\varphi(\omega)$, at the target. This is accomplished by scanning a well calibrated reference phase $f(\omega)$ and observing changes in the second harmonic spectrum. When the curvature of this function, $f''(\omega)$ corrects for the local phase distortion, $\varphi''(\omega)$, a local maximum appears in the second harmonic signal, thus allowing $\varphi''(\omega)$ to be mapped for the entire spectrum. From the integration of $\varphi''(\omega)$ the phase distortion can then be corrected. However for this work, the $\varphi''(\omega)$ information is sufficient as GVD is defined as

$$GVD(\omega) \equiv \frac{d}{d\omega}\left(\frac{1}{V_g(\omega)}\right) = \frac{d^2 k(\omega)}{d\omega^2} \equiv k''(\omega), \tag{1}$$

where $V_g(\omega)$ is the group velocity, $k(\omega) = (\omega/c)n(\omega)$ the wavenumber, and $n(\omega)$ the refractive index of the media, GVD can be obtained from differential MIIPS measurements performed with and without gas in a pressure cell. For a homogenous gas distribution, the phase difference is proportional to the path length in the cell, $\Delta\phi(\omega) = \Delta k(\omega)L$, and the GVD

$$GVD = \frac{\Delta(\phi''(\omega))}{L} = \frac{\phi''_{gas}(\omega) - \phi''_{vac}(\omega)}{L}, \tag{2}$$

where L is the interaction length with the dispersive media. A similar approach was previously demonstrated to provide GVD in solutions with high precision and accuracy [12]. Note that the MIIPS measurement yields GVD as a function of frequency, ω, i.e., it contains information concerning several leading orders of dispersion in the Taylor-series expansion near the carrier frequency ω_0

$$GVD(\omega) \equiv k''(\omega) = k''(\omega_0) + k'''(\omega_0) \cdot (\omega - \omega_0) + \ldots \qquad (3)$$

2. Experimental

The dispersion measurements were performed using an ultrabroadband femtosecond oscillator (Venteon; Pulse 1), operating at 75 MHz with 40 mW of average power. The spectral bandwidth covers over 400 nanometers, extending from 620 to 1050 nm (see Fig. 1). Such a broad spectrum allowed the measurement of dispersion across the entire 700–900 nm range without wavelength tuning. The output beam passed through a spatial filter and was then directed into a 4f reflective pulse shaper [13,14] (BioPhotonics Solutions Inc.; MIIPS Box 640) using a 640-pixel, dual-mask, liquid-crystal spatial-light modulator (SLM). Upon exiting the pulse shaper, the beam passed through one of two different pressure cells. One cell, with a path length of 0.90 m, was used for measurements in the low-pressure regime (1–4 bar) and was double passed, increasing the interaction length. The other cell had a path length of 0.20 m and was used for measurement in the high-pressure regime (10–50 bar). After exiting the pressure cell, the beam was focused onto a thin 10-μm KDP crystal for generation of the second harmonic. The second-harmonic-generation (SHG) signal was separated from the fundamental spectrum and focused into a spectrometer (Ocean Optics; QE65000).
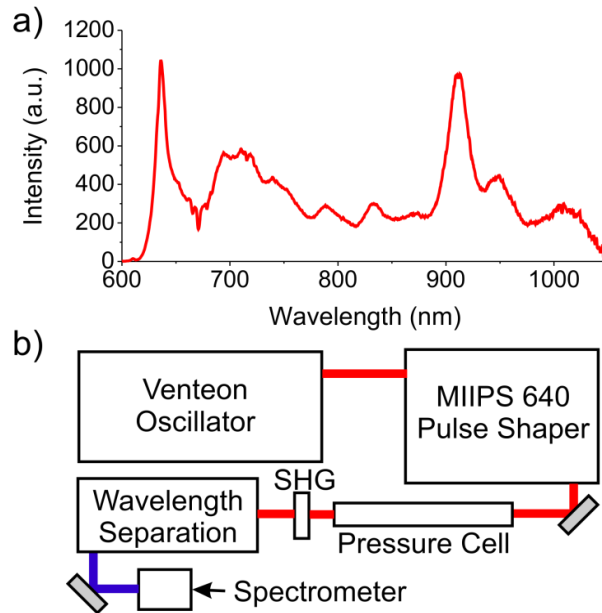

Fig. 1. (a) Broadband spectrum produced by the Venteon oscillator; (b) Diagram of experimental setup.

Prior to dispersion measurements, the cell was evacuated, and the intrinsic phase distortions to the system were measured and corrected using MIIPS. The sample gas was then introduced at the desired pressure, and MIIPS was again employed to measure the phase distortions produced by addition of the gas. For each gas measurement a pressure point was randomly selected, and the dispersion was measured in triplicate. All dispersion measurements were performed at room temperature (295 K).

3. Results

The results of low-pressure measurement of dispersion for seven cylinder gases are summarized in Fig. 2(a). For five of those gases, the dependence of dispersion on pressure was measured in a high-pressure regime as well [see Fig. 2(b)]. We found that for all gases, the dispersion changed linearly with pressure in the low-pressure regime, as expected due to direct pressure/density relationship (ideal gas behavior) in this limit. However, two of the measured gases–carbon dioxide and ethylene–exhibited a nonlinear dependence of GVD on gas pressure in the high-pressure regime.
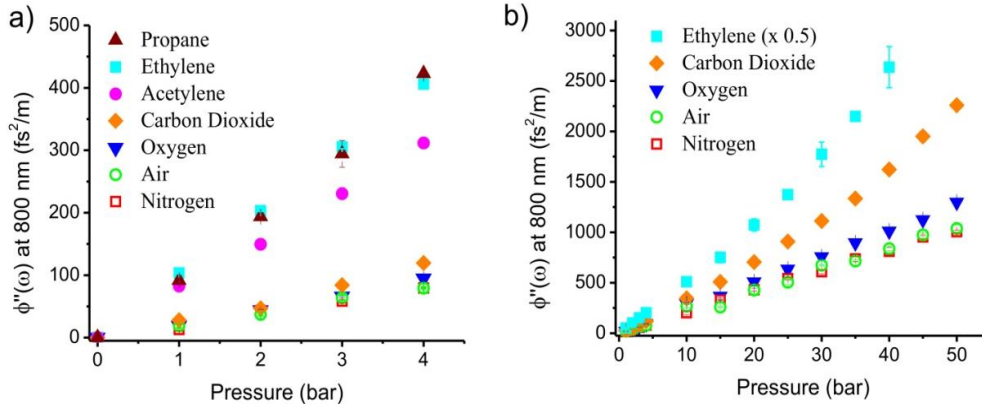

Fig. 2. Measured GVD at 800 nm as a function of pressure in (a) low (1−4 bar)- and (b) high (1−50 bar)-pressure regimes for several atmospheric and combustion-related gases.

The GVD of materials scales linearly with density. To illustrate this dependence for gases we obtain the density using the first approximation of the virial equation of state [15]

$$P = \rho RT \left[1 + \beta \rho \right] \qquad (4)$$

with the first virial coefficient (β), and plot dispersion as a function of gas density in Fig. 3. As expected we see the linear dependence on density.
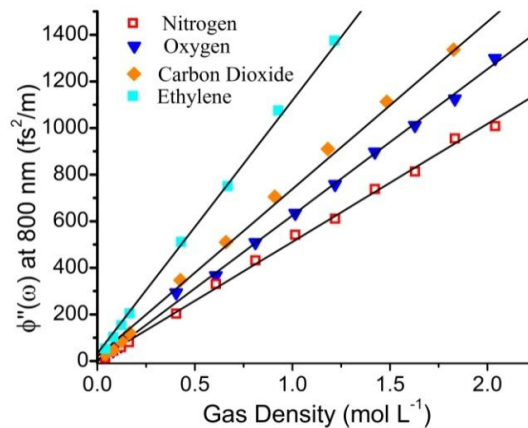

Fig. 3. Measured GVD at 800 nm as a function of gas density for nitrogen, oxygen, carbon dioxide, and ethylene along with linear fitting of the data.

For extracting the dispersion values of each gas or gas mixture, the rise of the second derivative of the phase with pressure within 1−4 bar (with 1-bar step) and for some gases

within 10–50 bar (with 5-bar step) is fitted by a linear function at every spectrometer wavelength. The measured dispersion is then normalized on the beam path length in the pressure cell and used to determine the second- and third-order dispersion coefficients by linear fitting of the data in the frequency domain, as shown in Fig. 4 for nitrogen.
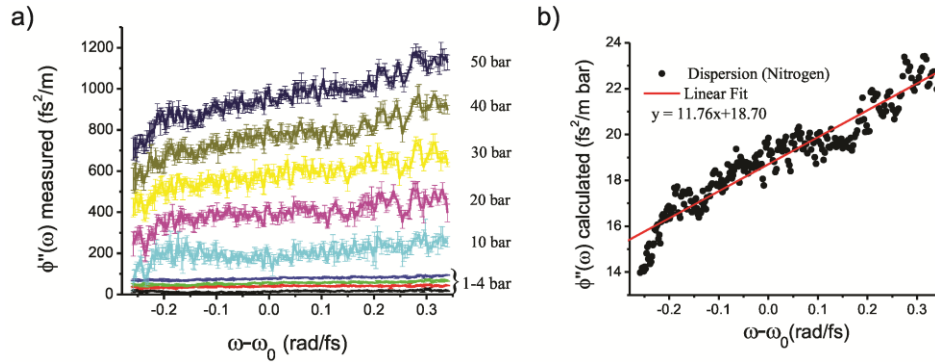

Fig. 4. (a) Measured dispersion for nitrogen (raw data) over the entire pressure range (data for some pressure values have been eliminated for clarity of presentation); (b) Dispersion of nitrogen normalized on path length and pressure, along with the linear fit. The intercept value provides the second-order coefficient, while the slope provides the third-order dispersion. The carrier frequency, ω_0, is set to 2.3526 rad/fs (λ_0 = 800.65 nm).

This analysis was performed for all measured gases. The experimental GVD curves and their linear fits are shown in Fig. 5. The retrieved second- and third-order dispersion coefficients are reported in Table 1 which contains the GVD coefficients for oxygen, nitrogen, and air that were obtained using the entire pressure range (1-50 bar). For carbon dioxide and ethylene, only the low-pressure (1–4 bar) data were used because of the nonlinearity at high pressures. The GVD of acetylene and propane was measured in the low-pressure (1–4 bar) regime only.
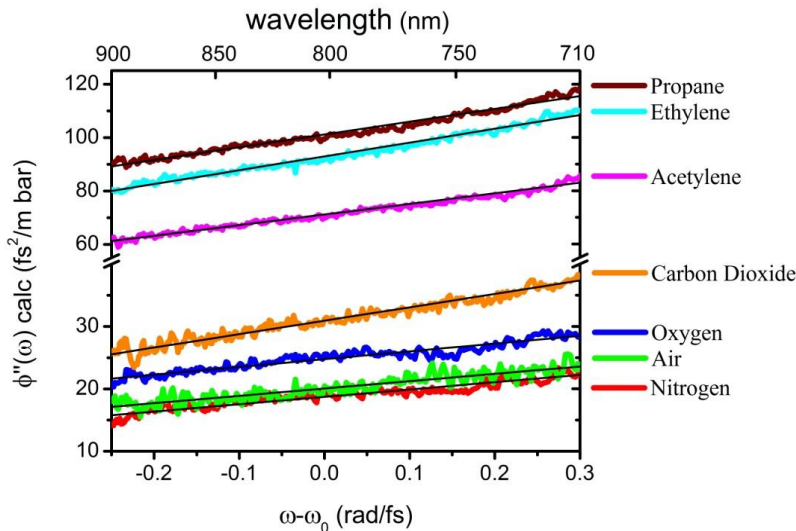

Fig. 5. Dispersion normalized on the path length and pressure for all the gases, along with the linear fit. For oxygen, nitrogen, and air, dispersion data from both pressure ranges are used; for all other gases only the low-pressure data, exhibiting linear pressure dependence, are used.

Table 1. Second- and Third-Order Dispersion Values at 800 nm for Each Gas at a Pressure of 1 Bar, along with the Standard Error in Fitting and the Statistics of the Linear Fit

Gas	Second-Order Dispersion (k''-fs^2/m)	Third-Order Dispersion (k'''-fs^3/m)	Coefficient of Determination (R^2)	Standard Deviation from the Linear Fit (fs^2/m)
Oxygen (O$_2$)	24.76 ± 0.04	12.5 ± 0.2	0.957	0.66
Nitrogen (N$_2$)	18.70 ± 0.04	11.8 ± 0.2	0.950	0.67
Air	20.05 ± 0.06	11.8 ± 0.4	0.906	0.89
Carbon Dioxide (CO$_2$)*	30.90 ± 0.05	21.5 ± 0.3	0.977	0.81
Acetylene (C$_2$H$_2$)*	78.20 ± 0.07	43.7 ± 0.4	0.989	1.12
Ethylene (C$_2$H$_4$)*	102.18 ± 0.08	57.0 ± 0.5	0.992	1.28
Propane (C$_3$H$_8$)*	111.21 ± 0.08	52.8 ± 0.5	0.990	1.30

*Values extracted from low-pressure data only.

To the authors' knowledge, most of these values have not been reported previously. The second-and third-order dispersion values of air, measured in [16–19], are in good agreement with our values (from ref. [16] 20.14 ± 0.14 fs^2/m and 18 ± 15 fs^3/m, respectively). Additional dispersion measurements have been made on several noble gases as well as nitrogen using interferometry; our measured values for nitrogen are also in agreement with these values (18.04 ± 0.15 fs^2/m and 10 ± 10 fs^3/m in [16]). Fitting of refractive index measurements with the Sellmeier equation [16] gives GVD values of 19.49 fs^2/m for nitrogen and 19.87 fs^2/m for air.

To highlight the role of dispersion in experiments where femtosecond pulses are used, we have examined the effect of dispersion on pulse-time duration by simulating the effect of various gas pressures in a 0.15-m-path-length pressure cell. The simulations were performed using the femtoPulse Master software (BioPhotonic Solutions Inc.), assuming Gaussian pulses with transform-limited (TL) time durations of 5, 10, and 50 fs. The software uses the input-pulse spectrum along with the second- and third-order dispersion values from Table 1 to calculate pulse durations at various pressures.

Gas Pressure (bar)	Oxygen (O_2)	Nitrogen (N_2)	Air	Carbon Dioxide (CO_2)	Ethylene (C_2H_4)	Acetylene (C_2H_2)	Propane (C_3H_8)
0	5	5	5	5	5	5	5
	10	10	10	10	10	10	10
	50	50	50	50	50	50	50
1	5.4	5.2	5.3	5.7	9.8	8.1	10.4
	11.4	11.4	11.4	11.5	11.7	11.6	11.8
	50	50	50	50	50	50	50
2	6.4	5.9	6	7.1	17.5	13.8	19
	11.5	11.5	11.5	11.5	12.9	12.2	13.2
	50	50	50	50	50	50	50
3	7.9	6.8	7	9.1	25.6	19.9	27.9
	11.6	11.5	11.5	11.7	15	13.4	15.7
	50	50	50	50	50	50	50
4	9.6	7.9	8.3	11.2	33.8	27.8	36.9
	11.7	11.6	11.6	11.9	18.1	15.1	19.4
	50	50	50	50	50.1	50	50.1
5	20.9	16.1	17.2	25.6	83.7	64.1	91.6
	13.6	12.6	12.8	15	41.5	32.0	45.3
	50.1	50	50	50.1	50.7	50.4	50.8
10	40.9	30.9	33.3	50.3	167.6	128.3	182.9
	21.2	17	17.9	25.8	82.7	63.4	90.2
	50.2	50	50.1	50.3	52.8	51.7	53.3
20	61.2	46	49.6	75.3	251	192.1	274.4
	30.6	23.7	25.2	37.8	124	94.9	135
	50.4	50.2	50.2	50.6	56.1	53.7	57.2
30	81.6	61	66	100.1	334.5	265	365.6
	40.5	30.8	33	49.9	165.3	126.4	180.2
	50.7	50.2	50.4	50.9	60.5	56.4	62.2
40	101.8	76.4	82.4	125.6	418	320.3	457.1
	50.2	38.1	40.9	62.4	206.6	158.3	225.4
	51	50.6	50.7	51.6	65.6	59.7	68.1

The simulation results indicate a significant temporal broadening of ultrashort pulses at high gas pressures–even for a 0.15-m path. From the values obtained it is obvious that the dispersion due to the gas component of an experimental setup is highly influential for short pulses at pressures typically used for combustion studies and must be taken into account–even at normal pressure conditions for distances of 0.5 m or longer. While the data in Table 2 may discourage one from using shorter laser pulses because of their greater propensity for dispersion, this can also be viewed as an advantage in the case of nonlinear spectroscopic applications, as discussed below.

When considering optical spectroscopy or imaging of high-pressure systems, the volume from which the optical signal emerges determines the spatial resolution of the measurement. Typically, three-dimensional sectioning capability in CARS diagnostics at range (i.e., with weakly focused beams) is achieved by crossing of two or more laser beams at a point of interest. Unfortunately, turbulence in the reacting-flow environment renders this cross-beam geometry very problematic. Single-beam spectroscopic imaging methods that have been developed recently [20,21] are much more immune to the inhomogeneity of the medium; however, another sectioning mechanism must be used to resolve the structure along the beam path. We have found that by implementing adaptive pulse compression to pre-chirp the laser pulses, the pulse can be adjusted to become TL at a specific location and, in turn, can be used to achieve spatial resolution along the weakly focused laser beam. Thus, the laser beam can be scanned to obtain an in-plane image, and the input pulse chirp can be tuned to adjust the depth.

This effect is examined in Fig. 6 for carbon dioxide at 2.24 mol·L^{-1} (corresponds to 40 bar at room temperature) by simulating the excitation efficiency of the Raman-active vibrational mode at 1285 cm^{-1}. It is assumed that the pulse energy is sufficiently small that transition saturation effects can be neglected. Pulse durations greater than 20 fs are not considered since they lack the spectral bandwidth to excite impulsively the 1285 cm^{-1} Raman mode. The input pulse energy is scaled to provide the same excitation efficiency at the zero Raman shift.

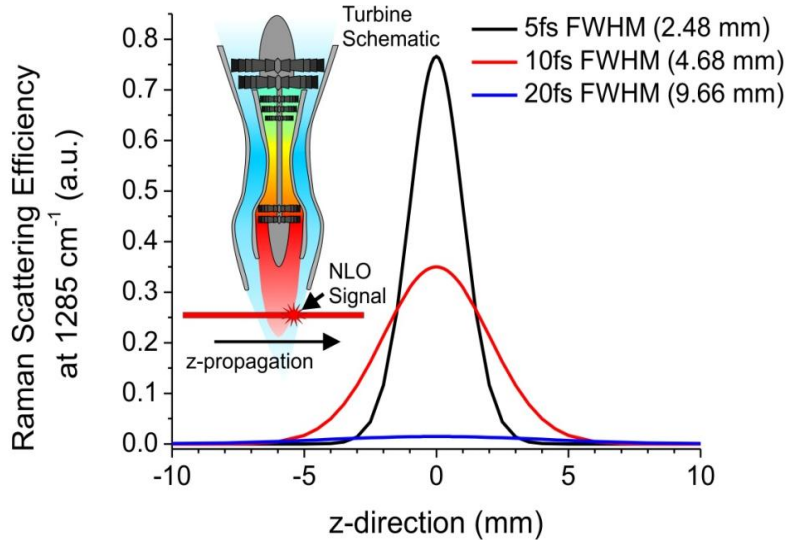Fig. 6. Simulated Raman scattering efficiency at 1285 cm^{-1} as a function of propagation distance CO_2 with a density of 2.24 mol·L^{-1}.The inset figure is a schematic example of how this improved spatial resolution can be used to select a region of interest to acquire data in a combustion process.

From the figure one can observe both the large increase in signal and the highly improved spatial resolution that results from the use of shorter pulses. The Raman excitation efficiency is directly related to the signal intensity in single-beam CARS measurements that employ a short pulse to provide the pump and stokes components and a long pulse as a probe. This illustrates the advantage of using very short pulses to perform single-beam CARS measurements. For a 5-fs pulse, one would obtain the full range of Raman shifts, along with a spatial resolution of ~2.5 mm along the z axis. The in-plane resolution is determined by the beam focusing and scanning parameters.

4. Conclusions

The increasing use of ultrafast laser systems and the greater availability of sub-30-fs laser sources have prompted the evaluation of pulse dispersion and its effects on nonlinear optical spectroscopy. An ultrabroadband laser source was used in this study to measure the spectral dispersion of a number of gases that are of importance to the combustion community. MIIPS was shown to be a straightforward approach for both accurately measuring the dispersion and introducing a pre-chirping phase mask that is capable of recovering TL pulses. It is suggested that dispersion, especially when using ultrabroadband laser sources, can provide a high level of axial resolution for single-beam spectroscopic methods. Such axial resolution is advantageous for obtaining three-dimensional images of flames.

Acknowledgments